Stable Measurement-Induced Floquet Enriched Topological Order

DinhDuy Vu[1,2], Ali Lavasani,[2] Jong Yeon Lee,[2] and Matthew P. A. Fisher[3]

[1]*Condensed Matter Theory Center and Joint Quantum Institute, Department of Physics, University of Maryland, College Park, Maryland 20742, USA*
[2]*Kavli Institute for Theoretical Physics, University of California, Santa Barbara, California 93106, USA*
[3]*Department of Physics, University of California, Santa Barbara, California 93106, USA*

The Floquet code utilizes a periodic sequence of two-qubit measurements to realize the topological order. After each measurement round, the instantaneous stabilizer group can be mapped to a honeycomb toric code, explaining the topological feature. The code also possesses a time-crystal order—the *e-m* transmutation after every cycle, breaking the Floquet symmetry of the measurement schedule. This behavior is distinct from the stationary topological order realized in either random circuits or time-independent Hamiltonian. Therefore, the resultant phase belongs to the overlap between the classes of Floquet enriched topological orders and measurement-induced phases. In this Letter, we construct a continuous path interpolating between the Floquet and toric codes, focusing on the transition between the time-crystal and stationary topological phases. We show that this transition is characterized by a divergent length scale. We also add single-qubit perturbations to the model and obtain a richer two-dimensional parametric phase diagram of the Floquet code, showing the stability of the Floquet enriched topological order.

Introduction.—Topological phases are highly interesting because their nonlocal integrals of motion are robust against local perturbations and thus beneficial for fault-tolerant quantum computation [1–5]. These exotic features were first established for the ground states of certain time-independent Hamiltonians such as $\mathbb{Z}_2$ toric code, and subsequently were extended to nonequilibrium unitary dynamics [6–11] as well as non-unitary dynamics that involve measurements [12–25]. In particular, Hasting and Haah proposed a circuit model consisting of a sequence of two-body measurements that gives rise to a dynamically generated quantum error correcting code which is closely related to $\mathbb{Z}_2$ toric code. Because of the time-periodic nature of the measurement sequence, the underlying code and logical operators transform periodically in time; thus the protocol code is called the Floquet code [23]. This code is not a stabilizer nor subsystem code, but dynamically generates logical qubits through a sequence of noncommuting measurements [23,26–28].

A remarkable characteristic of this class of Floquet codes is the time-crystalline ordering that transmutes magnetic (*m*) to electric (*e*)-type logical operators and vice versa each cycle. Unlike conventional time crystals that can be accessed by local order parameters [29–31], the *e-m* exchange can only be accessed from nonlocal operators, suggesting its topological nature. In fact, on an open boundary, this nontrivial exchange manifests as a radical chiral mode with a dynamical topological invariant $\sqrt{2}$ [32,33], and is thus dubbed as the Floquet enriched topological order (FET). The focus of this Letter is a measurement-induced version of FET.

The main goal of this Letter is to study the stability of the Floquet topological order against perturbations of the circuit model away from the ideal protocol in Ref. [23]. Although some ideas of fault tolerance have been discussed in [23], our Letter illuminates two aspects. First, it establishes the measurement-induced FET as a phase of matter, spanning a finite region of the parameter space. Second, for quantum platforms with native measurement operations, measurement-induced automorphisms of logical operators can be used as logical gates for quantum computing, e.g., the *e-m* exchange facilitated by the Floquet code is equivalent to a Hadamard gate that rotates between logical *X* and *Z*. Our Letter shows that such logical gates inherit the Floquet topological nature and are thus fault tolerant. For demonstration, we consider the effect of skipping some of the measurements as well as the effect of randomly replacing a two-qubit measurement with a pair of single-qubit measurements. Interestingly, by using an *error-corrected order parameter*, we find that the Floquet order is robust against small but finite perturbations, giving rise to an extended measurement-induced Floquet topological phase of matter. As one increases the perturbation strength, there is a measurement-induced phase transition to either a non-Floquet topological phase, a volume law phase, or a trivial area law phase (Fig. 1). We note that the FET phase, being stabilized by measurements, does not undergo thermalization in the long time limit. This is not the case for
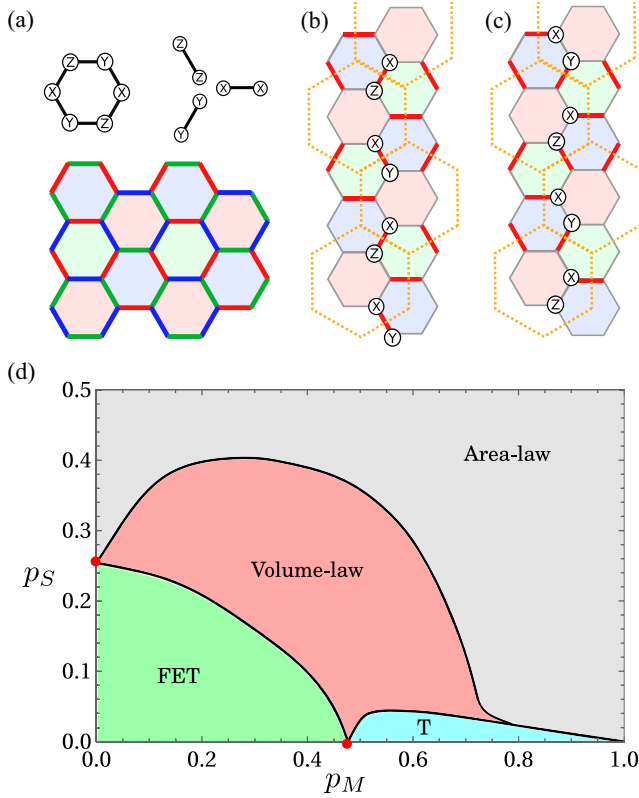
FIG. 1.   (a) Layout of the Floquet code with color labels for each link and plaquette and the explicit forms of the plaquette and link operators. The link operators only depend on the respective link orientation and not on the color. (b)–(c) One configuration of the m and e strings defined at the red round, respectively. (d) Phase diagram with respect to the missing p_M and single-qubit measurements p_S probabilities.

unitary models without either MBL [7–9,34,35] or pre-thermalization [36–38].

Model.—In this Letter, we consider a periodic-boundary $L \times L$ honeycomb lattice where a qubit is located at each vertex, with $2L^2$ qubits in total. Each hexagonal plaquette is assigned one of three colors: red, blue, or green, ensuring that no two adjacent plaquettes share the same color. Within this geometry, a link only connects plaquettes sharing the same color and thus inherits the respective color label. Furthermore, a two-qubit operator is assigned to each link, depending on the link orientation as demonstrated in Fig. 1(a). A plaquette operator is defined as the clockwise product of the link operators around the corresponding plaquette. For the standard Floquet code, all plaquette operators are going to have a definite value (either $+1$ or -1), and since they commute with all link operators, their value will not change in the subsequent steps.

Each link measurement projects a $\mathbb{C}^4$ Hilbert space of two adjacent physical qubits to a $\mathbb{C}^2$ Hilbert space which can then be regarded as a single effective qubit sitting on the link of a superlattice. Together with all the measured plaquette operators, these stabilizers make up a toric code

state on a hexagonal superlattice [23] (see Fig. 1). Note that an f logical operator is simply given by the product of all link operators along a nontrivial loop in the original lattice.

We consider two types of perturbations to the standard Floquet code. First we consider randomly missing link measurements at the blue and green rounds with probability $p_M < 1$, while the red round is free of missing defects. We refer to this perturbation as the "missing" (M) perturbation. Additionally, given that a link is measured, with probability p_S we replace the two-qubit measurement in the standard protocol with two disjoint single-qubit measurements, e.g, instead of measuring $X_1 X_2$ on a link, we measure X_1 on one end and X_2 on the other end. We denote this perturbation as the "single-qubit" (S) perturbation. This type of error is qualitative similar to random Pauli errors but simplified by the structure of the Floquet code [23]. M perturbations commute with all plaquette operators, leaving the quantum state always topological at the end of each measurement cycle. Meanwhile, S perturbations anticommute with the plaquettes and can drive the quantum state to a different phase.

We choose the initial state of the circuit to be the common eigenstate of all the plaquette operators and the logical operators m_x, m_z; and study the entanglement structure of the late time state of the circuit after $\sim \mathcal{O}(L)$ evolution. We note that due to the random dynamics of the circuit, the late time entanglement structure would be independent of the choice of the initial state [39]. Nevertheless, our choice of initial state optimizes the readout of the time-crystalline order and reduces the time for the quantum state to reach the topological sectors.

To obtain the phase diagram, we compute the tripartite mutual information (TMI) of the late time state averaged over different random realizations, which equals one in the topological phase, zero in the trivial area-law phase, and a negative extensive value in the volume-law phase [16,22,24,40]. The exact phase boundary can be obtained from a standard finite-size scaling method which also agrees with the transition in purification dynamics [40,41]. The detailed methodology and TMI data are presented in the Supplemental Material [39]. The phase diagram is shown in Fig. 1(d). Under the absence of S perturbations, i.e., $p_S = 0$, the diagram features a tricritical point at $p_M^c \approx 0.48$ which separates the FET phase with a period-doubled e-m exchange behavior from the stationary topological (T) phase for p_M strictly less than unity.

Missing link measurements.—First, we examine the phase diagram along the line $p_S = 0$ (no S perturbation). Because we have assumed no red link measurement would be missed, the bulk ISG is always the same (up to ± 1 signs) after each round of red link measurements. This leaves room for only the nonlocal logical qubits to have nontrivial dynamics. The limit $p_M = 0$ realizes a standard honeycomb Floquet code equipped with an e-m exchange every cycle. In
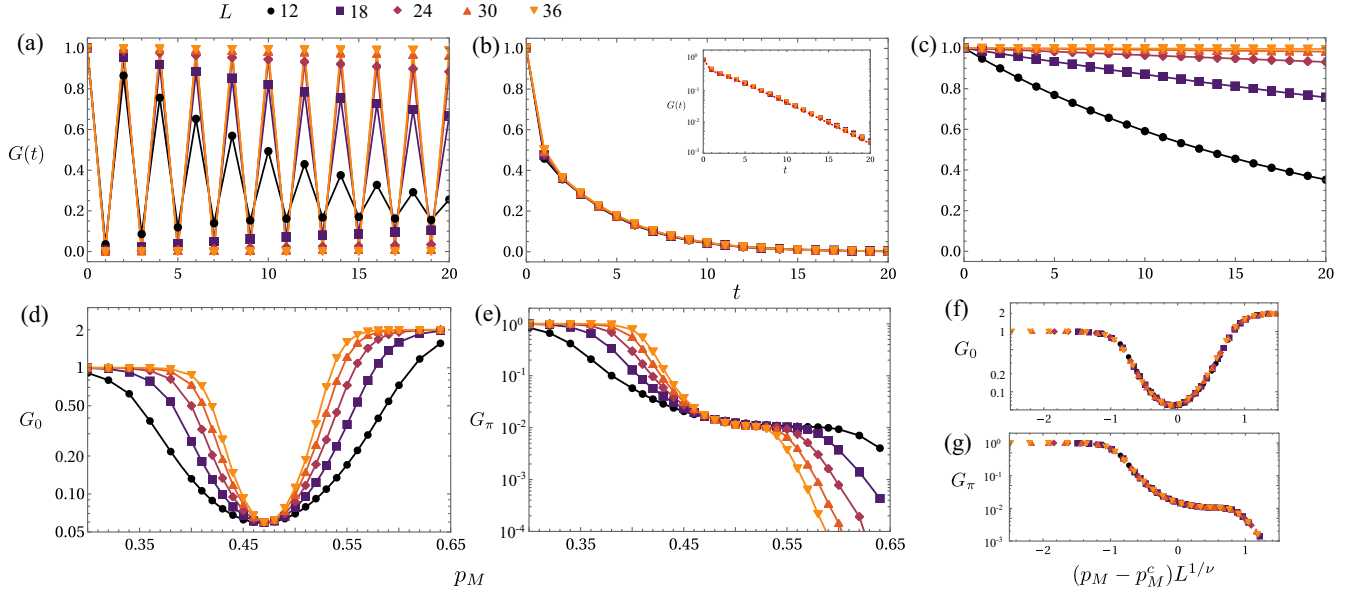
FIG. 2. (a)–(c) $G(t)$ for $p_M = 0.38$ (FET), 0.48 (critical), and 0.58 (T). The FET phase features double-period oscillations, which is lacking in the T phase. The inset of (b) shows $G(t)$ at the critical point fitted to a multichannel Markovian process. (d)–(e) The 0 and π components averaged over $T = 100$ cycles. (f)–(g) Data collapse of (d)–(e), respectively, with $(p_M^c, \nu) = [0.47(8), 1.36(0)]$ (f) and $[0.47(6), 1.35(4)]$ (g).

the opposite limit $p_M \to 1$, the other two color rounds are essentially absent and the circuit generates a stationary toric code topological order on the superlattice associated with the red links.

As we will show, the e-m exchange dynamics persists for $p_M > 0$ up to a critical value $p_M^c > 0$, after which it disappears and the system enters stationary toric code phase. To probe the Floquet dynamics, we consider the following procedure. Let m_x and m_z denote the m-type string operators winding around the torus along x and z directions, respectively. e_x and e_z are defined analogously to denote the logical e-type string operators. We start with the state which is the eigenstate of all plaquette operators as well as m_x and m_z. After every red round of measurements, we read out the expectation value of the m-loop along the x direction $G(t) = \overline{\langle m_x(t) \rangle^2}$, where the overline stands for averaging over random circuit realizations. For numerical simulation, we use Clifford formalism [42], where post-selection and averaging over measurement outcome are included. Note that for the initial state, we have $\langle m_x(0) \rangle = 1$ and $\langle e_x(0) \rangle = 0$. Therefore, due to the e-m exchange dynamics, we expect $G(t)$ to oscillate between 1 and 0 in the FET phase, while it should remain constant and equal to 1 in the toric code phase.

By inspecting $G(t)$ with varying $p_M \in [0, 1]$, we find an extended FET phase separated from the toric code topological phase by a sharp phase transition at $p_M^c = 0.48$. More specifically, for $p_M < p_M^c$, the value of $G(t)$ in odd and even cycles are visibly distinguishable, and $G(t)$ converges to the exact binary form $G(t) = (t + 1) \bmod 2$ as $L \to \infty$, signaling the time-crystalline order [Fig. 2(a)].

On the other hand, for $p_M > p_M^c$, $G(t)$ approaches a single-valued function $G(t) = 1$ in the thermodynamic limit [Fig. 2(c)]. Remarkably, at the critical point $p_M^c = 0.48$ which separates the two phases, $G(t)$ acquires a finite lifetime and follows a universal function independent of the system size [Fig. 2(b)], suggesting a zero dynamical exponent $z = 0$. This unusual z is due to the exact recovery of the bulk ISG after every cycle. Away from the $p_S = 0$ axis, the dynamic exponent returns to the conventional value of unity [39].

Accordingly, one can use the 0 and π components of the Fourier transform of $G(t)$ as order parameters for distinguishing the two phases and performing scaling analysis:

$$G_0 \equiv \lim_{T \to \infty} \frac{2}{T} \sum_{t=0}^{T} G(t), \quad G_\pi \equiv \lim_{T \to \infty} \frac{2}{T} \sum_{t=0}^{T} e^{i\pi t} G(t). \quad (1)$$

We note that the time limit should be taken after the thermodynamic limit, given that for any fixed system size, $\lim_{t \to \infty} G(t) = 0$ [see Figs. 2(a)–2(c)]. Figures 2(d)–2(e) shows the transition of these quantities across the critical point, taking $T = 100$; we have $G_0 = G_\pi = 1$ for $p_M < p_M^c$, while for $p_M > p_M^c$, we have $G_0 = 2$ and $G_\pi = 0$, in the thermodynamic limit. Both quantities follow the scaling form $F_{0,\pi}[(p - p_M^c)L^{1/\nu}]$ near the criticality, with $p_M^c \sim 0.48$ and $\nu \sim 1.35$–1.36 [see Figs. 2(e)–2(f)].

The nature of this phase transition can be understood by the microscopic dynamics of the Floquet phase. As is explained in Ref. [23], the color-wise measurement of the link operators along a loop maps the e-string along that

loop to an m-string along the same loop and vice versa (see also the Supplemental Material [39]). Therefore, whenever there exists a nontrivial path in the perturbed circuit model along which all link operators get measured in a cycle, the corresponding e-string operator along that path gets mapped to an m-string operator. However, due to the topological nature of the phase, it means *any* e-string operator maps to the corresponding m-string operator, as long as there exists one path along which all link operators get measured properly. This picture places the FET-T transition in the same universality class as 2D percolation. More specifically, given that red links are always measured, one can contract each red links into a point and consider the bond percolation problem on the resulting Kagome lattice. In fact, the critical value $p_M^c = 0.48$ for the FET-T phase transition agrees with the numerical estimate of bond percolation threshold on the Kagome lattice [43], which explains the extended FET phase for $p_M < p_M^c$. On the other hand, when $p_M > p_M^c$, there is no percolating path, and hence each cycle consists of only disconnected finite-size patches of measurements. Since such measurements cannot access logical information, the e-m exchange vanishes in the non-percolating phase. The percolation picture also explains why G_0 vanishes at $p_M = p_M^c$ [Fig. 2(d)]. At criticality, there is a finite chance of forming a percolating cluster whose boundary is also percolating around the torus. The result is a Markovian process that we show in the inset of Fig. 2(b) and explain in more detail in the Supplemental Material [39]. We note that the Markovian nature is lifted if red rounds are imperfect so that errors persist from one cycle to the next and accumulate with time. This is the case of the transition along the p_S axis in Fig. 1(d). Another option is to introduce M errors to red rounds. Both transitions are controlled by the 3D percolation universality [39], signifying the extension along the time direction.

Single-qubit measurements.—Even though the Floquet code measures closed f operators, these loops can be deformed into each other except for the two nontrivial loops winding around the torus and thus do not contribute to the entanglement inside the bulk. Therefore, the TMI stays exactly unity everywhere along the $p_S = 0$ axis. The picture changes significantly when we introduce single-qubit perturbations. In fact, the generators of the ISG after each red measurement round now contain "errors" to the Hasting-Haah protocol not found in the $p_S = 0$ case. In Fig. 3(a), we show an error generated by pair of red single-qubit measurements that can be detected through the two neighboring plaquettes with which this error anticommutes. Another type of errors occurs if more than one green or blue S perturbations happens along an f loop, resulting in open string errors that are not immediately transparent under plaquette measurements as shown in Fig. 3(b). We note that at the tricritical point, the circuit measures diverging f loops, which under nonzero p_S, break into extended strings. This explains the immediate emergence of
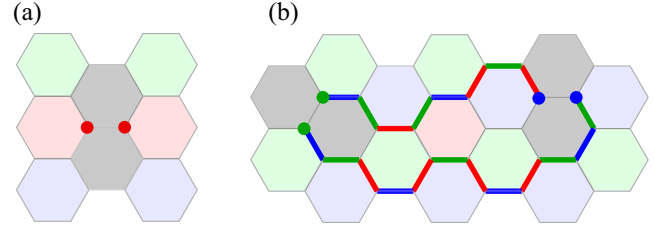

FIG. 3. Examples of errors that can occur to the ISG upon introducing S perturbations. (a) A local red S perturbation that can be detected through two adjacent plaquettes (gray). (b) Non-contractible open f string formed when at least two green or blue S perturbations intercept an f loop.

the volume phase at the critical point with any nonzero p_S shown in Fig. 1(d).

We expect that the FET characteristic must survive throughout the topological phase with $p_M < p_M^c$ as shown in Fig. 1(d) because there cannot be a continuous deformation between the FET and T phases. However, our previous probe cannot be applied straightforwardly in the presence of S perturbation because the string that we read out may randomly cross a point or an error string. Even worse, the probability of crossing an error string increases with system size, making the defined order parameter to vanish in the large-L limit. This is similar to the problem that the expectation values of loop operators decay exponentially with a perimeter law when the toric code Hamiltonian is subjected to an Ising field [5]. Nevertheless, the topological order or the ground state degeneracy is preserved and the exact 1-form symmetry characterizing the x loop is replaced by an emergent 1-form symmetry defined along a "fattened" loop with finite transverse width.

The same intuition can be applied to our model. Specifically, by deforming our m loop to avoid all the errors [see the inset of Fig. 4(a)], we can recover the finite-value order parameter as shown in Fig. 4. The exact implementation is described in the Supplemental Material [39]. The typical width d of the corrected m string is governed by the
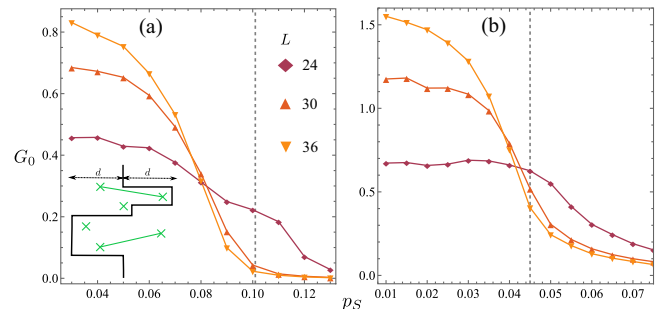

FIG. 4. The 0-component amplitude of G across the FET-volume-law transition at $p_M = 0.4$ (a) and the T-volume-law transition at $p_M = 0.55$ (b). The dash lines indicate the actual critical p_S obtained from TMI. The inset in (a) shows the corrected m string after being morphed to avoid all errors.

length of string errors, which is finite in the topological phase but grows with the system size in the volume-law phase. In our correction scheme, to be compatible with the finite size, we fix the maximum width as $d = 11$. Despite being independent of the system size in the area-law phase, d should increase as the circuit approaches the phase transition, so this d-fixing makes the apparent transition in Fig. 4 happen before the actual one computed from TMI; this is analogous to the situation where optimal and nonoptimal decoders perform similarly away from the phase boundaries in the circuit with measurements [44]. Nevertheless, this corrected order parameter justifies the robustness of the nontrivial e-m exchange against single-qubit perturbations, which is expected for a topological phase.

Conclusion.—We discover a robust Floquet topological phase in a quantum circuit characterized by a non-trivial exchange that brings the logical operator back to itself after two cycles. We establish in our quantum circuit model that this phase is stable against microscopic perturbations to the protocol, thus verifying the topological nature of the phase.

The research on Floquet topological order can advance in several directions. An outstanding question is the bulk invariant that can capture FET, which presumably describes a non-Abelian defect. Lastly, we note that our order parameter $G(t)$ is not linear in the density matrix, meaning that it can only be accessed experimentally with postselection. However, in principle, it should be possible to use the outcomes of the link measurements to perform proper error detection and error correction, similar to the standard Floquet code.

[1] E. Dennis, A. Kitaev, A. Landahl, and J. Preskill, J. Math. Phys. (N.Y.) **43**, 4452 (2002).

[2] A. Y. Kitaev, Ann. Phys. (N.Y.) **303**, 2 (2003).

[3] A. Kitaev and J. Preskill, Phys. Rev. Lett. **96**, 110404 (2006).

[4] M. A. Levin and X.-G. Wen, Phys. Rev. B **71**, 045110 (2005).

[5] M. B. Hastings and X.-G. Wen, Phys. Rev. B **72**, 045141 (2005).

[6] M. S. Rudner, N. H. Lindner, E. Berg, and M. Levin, Phys. Rev. X **3**, 031005 (2013).

[7] H. C. Po, L. Fidkowski, T. Morimoto, A. C. Potter, and A. Vishwanath, Phys. Rev. X **6**, 041070 (2016).

[8] A. C. Potter, T. Morimoto, and A. Vishwanath, Phys. Rev. X **6**, 041001 (2016).

[9] D. V. Else and C. Nayak, Phys. Rev. B **93**, 201103(R) (2016).

[10] M. S. Rudner and N. H. Lindner, Nat. Rev. Phys. **2**, 229 (2020).

[11] D. Vu, Phys. Rev. B **105**, 064304 (2022).

[12] Y. Li, X. Chen, and M. P. A. Fisher, Phys. Rev. B **98**, 205136 (2018).

[13] B. Skinner, J. Ruhman, and A. Nahum, Phys. Rev. X **9**, 031009 (2019).

[14] A. Chan, R. M. Nandkishore, M. Pretko, and G. Smith, Phys. Rev. B **99**, 224307 (2019).

[15] Y. Bao, S. Choi, and E. Altman, Phys. Rev. B **101**, 104301 (2020).

[16] A. Zabalo, M. J. Gullans, J. H. Wilson, S. Gopalakrishnan, D. A. Huse, and J. H. Pixley, Phys. Rev. B **101**, 060301(R) (2020).

[17] X. Chen, Y. Li, M. P. A. Fisher, and A. Lucas, Phys. Rev. Res. **2**, 033017 (2020).

[18] A. Lavasani, Y. Alavirad, and M. Barkeshli, Phys. Rev. Lett. **127**, 235701 (2021).

[19] Y. Bao, S. Choi, and E. Altman, Ann. Phys. (N.Y.) **435**, 168618 (2021).

[20] A. Lavasani, Y. Alavirad, and M. Barkeshli, Nat. Phys. **17**, 342 (2021).

[21] M. Wampler, B. J. J. Khor, G. Refael, and I. Klich, Phys. Rev. X **12**, 031031 (2022).

[22] A. Lavasani, Z.-X. Luo, and S. Vijay, Phys. Rev. B **108**, 115135 (2023).

[23] M. B. Hastings and J. Haah, Quantum **5**, 564 (2021).

[24] M. Ippoliti, M. J. Gullans, S. Gopalakrishnan, D. A. Huse, and V. Khemani, Phys. Rev. X **11**, 011030 (2021).

[25] A. Sriram, T. Rakovszky, V. Khemani, and M. Ippoliti, Phys. Rev. B **108**, 094304 (2023).

[26] D. Aasen, Z. Wang, and M. B. Hastings, Phys. Rev. B **106**, 085122 (2022).

[27] M. S. Kesselring, J. C. M. de la Fuente, F. Thomsen, J. Eisert, S. D. Bartlett, and B. J. Brown, Phys. Rev. B **108**, 094304 (2023).

[28] M. Davydova, N. Tantivasadakarn, and S. Balasubramanian, PRX Quantum **4**, 020341 (2023).

[29] D. V. Else, B. Bauer, and C. Nayak, Phys. Rev. Lett. **117**, 090402 (2016).

[30] V. Khemani, A. Lazarides, R. Moessner, and S. L. Sondhi, Phys. Rev. Lett. **116**, 250401 (2016).

[31] C. W. von Keyserlingk and S. L. Sondhi, Phys. Rev. B **93**, 245146 (2016).

[32] H. C. Po, L. Fidkowski, A. Vishwanath, and A. C. Potter, Phys. Rev. B **96**, 245116 (2017).

[33] A. C. Potter and T. Morimoto, Phys. Rev. B **95**, 155126 (2017).

[34] A. Lazarides, A. Das, and R. Moessner, Phys. Rev. Lett. **115**, 030402 (2015).

[35] D. A. Abanin, W. De Roeck, and F. Huveneers, Ann. Phys. (Amsterdam) **372**, 1 (2016).

[36] D. V. Else, B. Bauer, and C. Nayak, Phys. Rev. X **7**, 011026 (2017).

[37] D. Vu and S. D. Sarma, Phys. Rev. Lett. **130**, 130401 (2023).

[38] O. Hart and R. Nandkishore, Phys. Rev. B **106**, 214426 (2022).

[39] See Supplemental Material at http://link.aps.org/supplemental/10.1103/PhysRevLett.132.070401 for phase diagram of the Floquet honeycomb code and corrected order parameter in the presence of single-qubit perturbation.

[40] M. J. Gullans and D. A. Huse, Phys. Rev. X **10**, 041020 (2020).

[41] M. J. Gullans and D. A. Huse, Phys. Rev. Lett. **125**, 070606 (2020).

[42] S. Aaronson and D. Gottesman, Phys. Rev. A **70**, 052328 (2004).

[43] R. M. Ziff and P. N. Suding, J. Phys. A **30**, 5351 (1997).

[44] J. Y. Lee, W. Ji, Z. Bi, and M. P. A. Fisher, arXiv:2208.11699.